RSC Advances

PAPER

View Article Online
View Journal | View Issue

Cite this: *RSC Adv.*, 2016, **6**, 104549

Green fabrication of magnetic recoverable graphene/$MnFe_2O_4$ hybrids for efficient decomposition of methylene blue and the Mn/Fe redox synergetic mechanism†

Xiyue Peng,[a] Jiangying Qu,*[ab] Shuo Tian,[a] Yanwei Ding,[a] Xi Hai,[a] Bo Jiang,[c] Mingbo Wu*[c] and Jieshan Qiu[b]

Received 30th September 2016
Accepted 11th October 2016

DOI: 10.1039/c6ra24320g

www.rsc.org/advances

Herein, we report an environmentally benign synthesis of a high-performance reduced graphene oxide/$MnFe_2O_4$ (RGO/$MnFe_2O_4$) catalyst for methylene blue (MB) decomposition in neutral solution using a GO/$MnSO_4$ suspension from a modified Hummers method and $FeSO_4$ as the precursors. The as-prepared RGO/$MnFe_2O_4$ catalyst shows exceptional performance towards the MB decomposition in the presence of H_2O_2. In particular, 10 mL of MB (50 mg L^{-1}) can be thoroughly decolorized in 130 min and 78% mineralized with 5 mg of RGO/$MnFe_2O_4$ hybrid at room temperature. More interestingly, the catalysts can be magnetically recycled. The good catalytic performance of the RGO/$MnFe_2O_4$ hybrid is not only attributed to the synergetic effects of RGO, $MnFe_2O_4$, H_2O_2 and MB molecules, but also related to the redox couples of Fe/Mn ions during the reaction. We have firstly experimentally demonstrated that the catalytic performance of $MnFe_2O_4$ is dominated by Fe^{3+}/Fe^{2+} in the initial stage (<70 min) then by Mn^{3+}/Mn^{2+} in the later stage (>70 min), while Fe^{2+}/Mn^{3+} redox in turn benefits the redox cycles of Fe^{3+}/Fe^{2+} and Mn^{3+}/Mn^{2+}. Our results not only provide an alternative strategy for green synthesis of high-performance functional nanomaterials, but also promote a deep understanding of the mechanism of $MnFe_2O_4$ catalyst for MB decomposition.

Introduction

An ever increasing amount of toxic and hazardous waste water is being generated from industries and consequently results in serious environmental issues.[1–3] Organic dyes are a major type of pollutant widely existing in nature water, and thus the development of powerful and practical methods for the degradation of organic dyes has attracted world-wide attention.[4] As an effective advanced oxidation technology, catalysts employing the traditional homogeneous Fenton reaction with free Fe^{2+} have been widely used to decompose organic dyes. However, the narrow pH range (pH 2–3) and the polluted iron sludge generated at the end of process prohibit the practical application of this technology.[5,6] To overcome these drawbacks, potential applications of heterogeneous Fenton-like catalysts have been investigated widely. Specifically, iron based Fenton-like catalysts such as Fe_3O_4, Fe_2O_3, FeOOH[7–9] and manganese based ones such as MnO_2, Mn_3O_4 (ref. 10 and 11) are two common kinds of heterogeneous catalysts for the degradation of organic dyes. Nevertheless, the catalytic performance of these mono-metal oxide catalysts is far from satisfaction. Furthermore, the recycling of these heterogeneous catalysts as another crucial issue needs to be addressed (except for Fe_3O_4 and γ-Fe_2O_3, δ-FeOOH).[4] The introduction of Mn into the structure of Fe_3O_4 to produce magnetic Mn–Fe bimetal oxide catalyst provides new route for the enhancement of Fenton activity.[12–14] In this field, $MnFe_2O_4$ particles have been intensively investigated mainly because of their high activity, good magnetization, nice biocompatibility and low cost.[15,16] For example, Fang *et al.* synthesized coated $MnFe_2O_4$ nanocomposites for the decomposition of Red X-3B with the assistance of microwave.[17] Yang *et al.* prepared the magnetic $MnFe_2O_4$ as the adsorbent for the removals of methylene blue (MB) and Congo red in single and binary dye systems.[18] Despite these advances, the unique magnetic property of $MnFe_2O_4$ particles usually leads to their aggregation, thus decreasing their catalytic efficiency.[19] As a result, extensive efforts have to be made in controlling the size and dispersion of $MnFe_2O_4$ particles for enhanced catalytic performance.

[a]*Faculty of Chemistry and Chemical Engineering, Liaoning Normal University, Dalian, 116029, China. E-mail: qujy@lnnu.edu.cn; Tel: +86-411-82158329*

[b]*Carbon Research Laboratory, Center for Nano Materials and Science, School of Chemical Engineering, State Key Lab of Fine Chemicals, Dalian University of Technology, Dalian, 116024, China*

[c]*State Key Laboratory of Heavy Oil Processing, School of Chemical Engineering, China University of Petroleum, Qingdao, 266580, China. E-mail: wumb@upc.edu.cn; Tel: +86-532-86983452*

† Electronic supplementary information (ESI) available. See DOI: 10.1039/c6ra24320g

Graphite and graphene are two common carbon materials for fabricating nanocomposites.[20,21] The former exhibits significant potential in the improvement of thermal conductivities of the composites.[22,23] However, the later with unique electronic property, large surface area, high chemical stability and good mechanical flexibility can not only serve as an ideal substrate for growing functional nanoparticles, but also as a charge transfer medium in the catalytic reactions.[24–26] Nowadays, it is demonstrated that magnetic heterogeneous catalysts can be uniformly dispersed on graphene to fabricate the hybrids towards the degradation of water pollution.[27] For example, Bai *et al.* fabricated graphene/$MnFe_2O_4$ hybrids from GO, Fe^{2+} and Mn^{2+}, which could remove over 75% rhodamine B and 95% MB within 180 min.[28] Using the similar method, Yao's group demonstrated that magnetic graphene/$MnFe_2O_4$ exhibited 97% degradation of MB in 120 min with the assistance of peroxymonosulfate, which was much higher than that of bare $MnFe_2O_4$.[29] These studies indicate that the combination of graphene with magnetic $MnFe_2O_4$ provides the potential catalytic route which meets the requirements of high catalytic activity, easy recovery and reuse. However, the common methods for the fabrication of graphene/$MnFe_2O_4$ catalysts often begin with GO as the precursor and additional Mn^{2+} ions as Mn source. Generally, GO produced by the modified Hummers method requires intercalation and oxidation of graphite with a stoichiometric amount of $KMnO_4$ and H_2SO_4 and results in a large amount of waste containing H^+, Mn^{2+} and SO_4^{2-} ions.[30,31] For the viewpoint of the whole synthesis, the production of RGO/$MnFe_2O_4$ will be more valued if the H^+, Mn^{2+} and SO_4^{2-} ions can be fully utilized, which will not only avoid the tedious purification process of GO as well as the production of large amount of waste, but also contribute to highly atom-economic synthesis.[32] We previously fabricated reduced graphene oxide/MnO_2 (RGO/MnO_2) and GO/Mn_3O_4 composites with GO/$MnSO_4$ suspension as Mn source and the resultant samples exhibited good catalytic performances for 100% degradation of MB in 5 min at 50 °C and 200 min at room temperature, respectively.[31,32] In spite of our efforts, the enhanced catalytic activity, facile recycling treatment and further understanding of the catalytic mechanism are desired.

It is widely reported that hydroxyl radical ($^{\bullet}OH$) radical is crucial parameter for understanding the effective degradation of dyes with H_2O_2 assisted heterogeneous Fenton-like reaction.[12] In principle, H_2O_2 activation mechanism is critically depends on the nature of the catalyst. The mono-metal catalyst such as iron oxide, manganese oxide with multiple redox states to activate H_2O_2 into $^{\bullet}OH$ has been widely studied.[15,29] However, the exact role of oxidation state of different components for bimetal oxide catalyst during Fenton reaction needs to be further explored based on the experimental data.

In this work, we further develop environmentally benign synthesis of magnetic RGO/$MnFe_2O_4$ hybrids from the pristine suspension (GO/$MnSO_4$) with the addition of $FeSO_4$ as the iron source. The work provides the effective utilization of Mn^{2+} ions in the pristine suspension of GO/$MnSO_4$, and the introduction of RGO can facilitate the dispersion of the *in situ* formed magnetic particles, *via* which their aggregation is significantly alleviated. Due to these structural merits, the as-prepared hybrids show improved catalytic performance towards the MB decomposition in the presence of H_2O_2. In addition, these catalysts can be facilely recycled due to the magnetic property of the $MnFe_2O_4$ nanoparticles. More importantly, the roles of the oxidation state of Fe(III)/Mn(II) in $MnFe_2O_4$ with varied redox property (Fe^{3+}/Fe^{2+}, Mn^{3+}/Mn^{2+} and Fe^{2+}/Mn^{3+}) on the catalytic performance and the involved mechanism are investigated in detail.

Experimental

Synthesis of RGO/$MnFe_2O_4$ hybrids

The procedure for the synthesis of RGO/$MnFe_2O_4$ hybrids was carried out as follows. First, 10 mL of the homogeneous GO/$MnSO_4$ suspension (13 mg mL^{-1} GO and 0.22 mol L^{-1} $MnSO_4$), which was synthesized by modified Hummers method according to ref. 32 and 33, was sonicated for 20 min. Then 1.22 g $FeSO_4 \cdot 7H_2O$ was added and the mixed suspension was stirred at room temperature. Subsequently, 2 mol L^{-1} KOH was added into the above solution for another 0.5 h under bubbling air and stirring until the pH = 12. The system was then transferred in a 20 mL Teflon-lined autoclave at 150 °C for 15 h. Finally, the black precipitate (RGO/$MnFe_2O_4$) was collected by filtration, washed thoroughly with distilled water, and fully dried at 80 °C over night.

RGO/$MnFe_2O_4$ hybrids with different mass contents of $MnFe_2O_4$ were synthesized by tailoring the ratio of GO/$MnSO_4$ to $FeSO_4$. First, GO/$MnSO_4$ suspensions with different mass ratios of GO to $MnSO_4$ were prepared according to ref. 33. Then, a certain amount of $FeSO_4 \cdot 7H_2O$ was added into the above suspension based on the theoretic molar ratio of Fe^{2+} to Mn^{2+} in the $MnFe_2O_4$ molecule, which was accurately equal to be 2 : 1. The following steps by adding KOH and other procedures are similar to the above process. The resultant samples were named as RGO/$MnFe_2O_4$-*X*, where *X* represented the mass percentage of $MnFe_2O_4$ in RGO/$MnFe_2O_4$ hybrids. For comparison, RGO or bare $MnFe_2O_4$ particle were prepared in a similar way in the absence of $MnFe_2O_4$ or GO.

Test of the catalytic performance

The activities of RGO/$MnFe_2O_4$ hybrids for the decomposition of MB dye were investigated. In a typical test, 5 mg of the resulting catalyst and a solution which contained 10 mL of MB dye solution (50 mg L^{-1}) as well as 5 mL of H_2O_2 (30 wt%) solution were mixed under continuous stirring. The concentration of MB dye was determined by UV-vis spectroscopy at 664 nm. Besides, the catalyst was magnetically separated and reused in a fresh MB and H_2O_2 solution after completion of the reaction for the stability tests of RGO/$MnFe_2O_4$-75. Furthermore, the formation of active $^{\bullet}OH$ upon irradiation was chosen to evaluate the catalytic properties of the RGO/$MnFe_2O_4$ hybrids by using terephthalic acid (TA) as the probe molecule. The detailed process of catalytic activity test and the $^{\bullet}OH$ analysis were shown in ESI Sp1 and Sp2,† respectively.

The structure analyses and catalytic measurements of the obtained samples were similar to our previous report.[32]

Results and discussion

The characterization of RGO/$MnFe_2O_4$ hybrids

The environmentally benign synthesis of magnetic RGO/$MnFe_2O_4$ catalyst for the decomposition of MB is illustrated in Fig. 1. Firstly, we took full use of the pristine GO/$MnSO_4$ suspension (13 mg mL^{-1} GO and 0.22 mol L^{-1} $MnSO_4$) derived from a modified Hummers method,[34,35] in which Mn^{2+} ions preferably combined with the O atoms of the negatively charged surface of GO sheets *via* electrostatic interaction.[36] Additional $FeSO_4$ and KOH were successively added into the system. After being hydrothermally treated at 150 °C for 15 h, $MnFe_2O_4$ was formed ($2Mn^{2+} + 12OH^- + 4Fe^{2+} + O_2 = 2MnFe_2O_4 + 6H_2O$) and anchored firmly on the RGO surface to form RGO/$MnFe_2O_4$ hybrids. Moreover, the only by-product, namely, K_2SO_4, could be recycled for other purposes (ESI Sp3†). The resultant RGO/$MnFe_2O_4$ hybrids showed effective catalytic decomposition of MB and could be magnetically recovered.

The powder X-ray diffraction (XRD) patterns of RGO/$MnFe_2O_4$-75, bare $MnFe_2O_4$ particles and RGO were shown in Fig. 2a. $MnFe_2O_4$ particles exhibit the intense peaks corresponding to (220), (311), (400), (511) and (440) planes, which match well with the standard $MnFe_2O_4$ (JCPDS 38-0430).[17] For RGO/$MnFe_2O_4$-75, the intense peaks are weaker than those of bare $MnFe_2O_4$, which may be attributed to the small size and good distribution of $MnFe_2O_4$ in the hybrid. Furthermore, RGO/$MnFe_2O_4$-75 and RGO show the broad and weak peak at around $2\theta = 25°$ as the result of the hydrothermal reduction of GO to RGO.[29]

The Raman spectra of the obtained samples were shown in Fig. 2b. It is well known that the G band at 1596 cm^{-1} is usually assigned to sp^2 carbon domains, while the D band located at 1345 cm^{-1} is associated with the defects and disorder carbon in the graphitic layers.[31,36] The intensity ratio of D band to G band (I_D/I_G) is usually used as the measure of the ordering quality of carbon materials. A lower intensity I_D/I_G ratio of RGO/$MnFe_2O_4$-75 hybrid, *i.e.*, 1.11 is observed compared with 1.34 of RGO, suggesting that $MnFe_2O_4$ in RGO/$MnFe_2O_4$-75 can help to increase the size of the sp^2 domains. In addition, the characteristic peak at 612 cm^{-1} of RGO/$MnFe_2O_4$-75 matches completely with that of bare $MnFe_2O_4$ particles.[29,37]

XPS analysis was further employed to elaborate the surface chemical bonding states of the RGO/$MnFe_2O_4$ hybrid. The full-scale XPS spectra with C 1s, O 1s, Mn 2p, and Fe 2p spectra were shown in Fig. 3a. The spectrum of Fe 2p (Fig. 3b) has two main peaks at binding energies of 711.3 and 725.1 eV, which are related to Fe $2p_{3/2}$ and Fe $2p_{1/2}$, respectively. The satellite peaks at the position of 719.8 and 733.3 eV are also visible, confirming the presence of Fe^{3+} chemical state within $MnFe_2O_4$.[29,38] As shown in Fig. 3c, it is found that the XPS spectrum of Mn 2p presents two main peaks of Mn $2p_{3/2}$ (641.2 eV) and Mn $2p_{1/2}$ (652.8 eV) together with a satellite peak (644.9 eV), which are in good agreement with the Mn^{2+} chemical state.[39,40] The C 1s peak at 284.6 eV is commonly assigned to the elemental carbon (Fig. 3d).[41] When comparing to the peaks of GO (the inset in Fig. 3d), the C–C/C=C peak becomes predominant (284.6 eV) while the peaks of C–O and C=O decrease drastically. This means that GO has been reduced to RGO except for a small amount oxygen-containing groups after being hydrothermally treated, which agrees with the XRD result.

SEM images of RGO/$MnFe_2O_4$-75 and bare $MnFe_2O_4$ were shown in Fig. 4. Sandwich-like RGO layers are decorated by $MnFe_2O_4$ spheres with the size of around 200 nm, indicating that the presence of RGO effectively inhibits the aggregation of $MnFe_2O_4$ particles (Fig. 4a and b). Meanwhile, the existence of $MnFe_2O_4$ can prevent RGO from stacking.[42] Such synergistic interaction plays a positive role in the catalytic decomposition of organic pollutants due to the improved transportation of electrons between $MnFe_2O_4$ and RGO.[30] For comparison, the bare $MnFe_2O_4$ particles (Fig. 4c) with diameters ranging from 100 to 500 nm seriously aggregated in the absence of RGO.

TGA was applied from room temperature to 700 °C in air flow to analyze the thermal stability and quantified composition of RGO/$MnFe_2O_4$ hybrids. As shown in Fig. 5a, the gradual weight

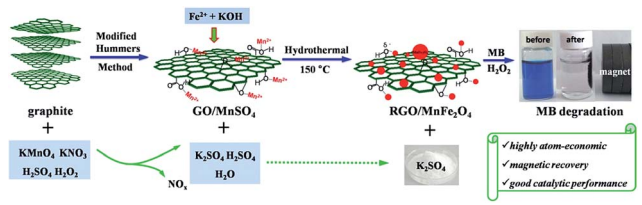

Fig. 1 Schematic synthesis of magnetically recoverable RGO/$MnFe_2O_4$ hybrids for the decomposition of MB dye.

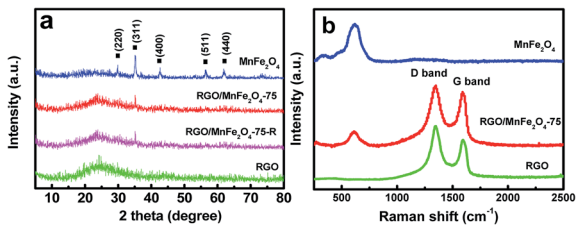

Fig. 2 (a) XRD patterns and (b) Raman spectra of RGO/$MnFe_2O_4$-75, $MnFe_2O_4$, and RGO.

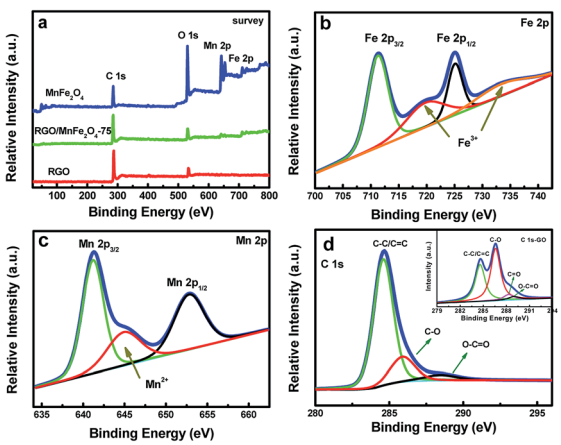

Fig. 3 XPS spectra of RGO/$MnFe_2O_4$-75, $MnFe_2O_4$ and RGO: (a) the survey scan; (b–d) Fe 2p region, Mn 2p region and C 1s region of RGO/$MnFe_2O_4$-75; the inset in (d) is C 1s region of GO.

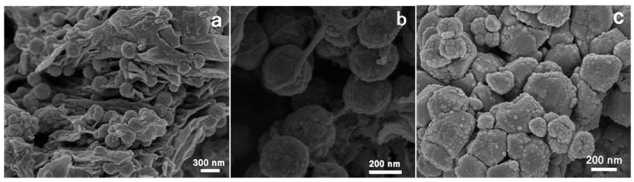

Fig. 4 SEM images of (a and b) RGO/$MnFe_2O_4$-75 and (c) the bare $MnFe_2O_4$.

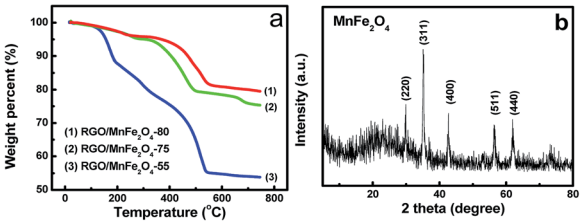

Fig. 5 (a) TGA curves of RGO/$MnFe_2O_4$ hybrids with different $MnFe_2O_4$ contents and (b) XRD pattern of residual $MnFe_2O_4$ after the burning of RGO of RGO/$MnFe_2O_4$-75.

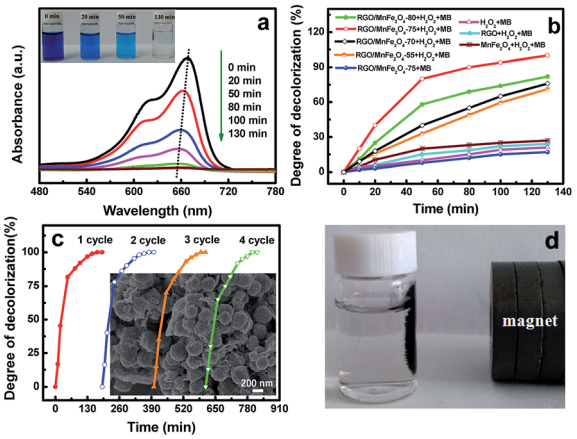

Fig. 6 (a) Absorption spectra of MB solution (50 mg L^{-1}, 10 mL) of RGO/$MnFe_2O_4$-75 hybrid in different time intervals (the inset is the photo image); (b) time profiles of MB decomposition under different conditions; (c) the decomposition of MB with RGO/$MnFe_2O_4$-R, the inset is its SEM image; (d) the photo image of magnetically recyclable RGO/$MnFe_2O_4$.

loss in RGO/$MnFe_2O_4$-75 hybrid occurs at 20–500 °C, which is corresponding to the loss of the physically adsorbed water and the burning of RGO.[31] At last, $MnFe_2O_4$ with the mass percent of 75% is left after RGO is fully burned up at 700 °C (evidenced by XRD analysis in Fig. 5b). Therefore, it is calculated that the content of $MnFe_2O_4$ in RGO/$MnFe_2O_4$ is 75%. The mass ratios of $MnFe_2O_4$ in RGO/$MnFe_2O_4$ with 80% and 55% can be further tuned by adjusting the weight ratio of pristine GO/$MnSO_4$ suspension to $FeSO_4$ (shown in Experimental Section).

Catalytic activities and stability test of RGO/$MnFe_2O_4$ hybrids

The catalytic activities of the as-prepared samples were evaluated at a given reaction interval in the presence of H_2O_2. The UV-vis absorption spectra of MB solution treated by RGO/$MnFe_2O_4$-75 hybrid were shown in Fig. 6a. The two characteristic absorption peaks appearing at 614 and 664 nm are contributed to the typical MB peaks in visible region at the starting solution.[43] After adding both RGO/$MnFe_2O_4$-75 and H_2O_2, the absorption peaks of MB solution obviously decrease. It can be seen that the absorption of MB is relatively rapid in the initial 50 min and its gradual blue shift is observed with prolonged reaction time, indicating the breakdown of chromophore structure of MB.[32] As a result, the solution turns colorless gradually within 130 min and the corresponding photo images were shown in the inset of Fig. 6a. A series of comparative experiments were designed to verify the catalytic performance of the obtained samples. Fig. 6b shows the result of the decomposition degree of MB dye within 130 min for different samples. For comparison, the degree of MB decolorization is 21% without catalyst (only MB and H_2O_2), which is slightly higher than 17.3% in the absence of H_2O_2 (only MB and RGO/$MnFe_2O_4$-75) because of the low specific surface area (29 $m^2\ g^{-1}$) of RGO/$MnFe_2O_4$-75 hybrid. Therefore, the synergetic effect of catalyst and H_2O_2 plays an important role in efficient decomposition of MB dye from water. To further explore the synergistic effect of $MnFe_2O_4$ and RGO in RGO/$MnFe_2O_4$ hybrids, the catalytic activities of RGO/$MnFe_2O_4$ with different $MnFe_2O_4$ contents as well as pure RGO in the decomposition of MB were compared. It is found that 27% and 24% of MB are decolorized by bare $MnFe_2O_4$ particles and RGO, respectively. As the mass ratio of $MnFe_2O_4$ in RGO/$MnFe_2O_4$ hybrids varies from 55 to 75 wt%, the decolorization degree of MB increases from 71.2 to 100% within 130 min, which is more effective than that of the reported RGO/$MnFe_2O_4$ hybrid (95% MB decomposition within 180 min)[28] and our previous work on RGO/MnO_2 and GO/Mn_3O_4 compositions (100% MB decomposition within 5 min at 50 °C and 200 min at room temperature, respectively).[31,32] The further increased $MnFe_2O_4$ content to 80 wt%, however, results in a low MB decolorization rate of 82% under the same condition. Thus, 75 wt% is the best content for $MnFe_2O_4$ in RGO/$MnFe_2O_4$ hybrid for MB decolorization. The mechanism of the significant activity enhancement of RGO/$MnFe_2O_4$ hybrids is illustrated as below. First, RGO can prevent the aggregation of $MnFe_2O_4$ particles as well as serve as the electron transfer bridges to enhance the MB decomposition based on the XRD, Raman and SEM analyses. Considering 2D planar structure and giant π-conjugation system of RGO, the MB molecules can be adsorbed on the surface of RGO and retained in close proximity to the active sites of $MnFe_2O_4$, thus providing great opportunities to degrade the contaminants.[44] Second, the uniformly dispersed $MnFe_2O_4$ particles can increase the number of active sites for the catalytic decomposition of MB as well. Besides, Mn^{2+} also plays an important role in accelerating the electron transfer process between Fe^{2+}/Fe^{3+}, and thus improves the catalytic activity to some extent,[45,46] which will be discussed in the following part.

Undoubtedly, the stability of the catalyst is quite important for practical applications. Thus, the stability test of RGO/$MnFe_2O_4$-75 is shown in Fig. 6c. Four recycling runs of RGO/$MnFe_2O_4$-75 were performed without any noticeable loss of

catalytic ability. The catalyst named as RGO/$MnFe_2O_4$-75-R which was recovered after the test was further studied by SEM (the inset of Fig. 6c) and XRD analyses (Fig. 2a), which indicates that the size, morphology, and structure of the catalysts remains almost unchanged, further demonstrating their excellent stability. The concentration of the slightly leached Mn ions (about 0.5 wt%) from RGO/$MnFe_2O_4$-75 was further detected by inductive coupled plasma emission spectrometer (ICP),[32] indicating the excellent stability of RGO/$MnFe_2O_4$-75 hybrid. It's worth mentioning that the catalyst can be completely recovered with a permanent magnet after each run (as shown in Fig. 6d), which not only simplifies operation steps and improves working efficiency, but also meets the demands of green chemistry.

As is known to all, the SO_4^{2-} mineralization is widely used to evaluate the MB degradation efficiency.[31] In this work, the SO_4^{2-} concentration in the final solution was measured to be 7.1 mg L^{-1} (0.4 mg L^{-1} of the SO_4^{2-} comes from the H_2O_2 reagent). According to the theoretically calculated concentration (about 8.5 mg L^{-1}) after 100% decolorization of MB by RGO/$MnFe_2O_4$-75, we draw the conclusion that MB dye has been effectively decolorized and about 79% has been mineralized over RGO/$MnFe_2O_4$-75 hybrid, which is higher than those of previously reported GO/Mn_3O_4 composite (77%),[32] RGO/MnO_2 composite (66%)[31] and Mn_3O_4/graphene hybrid (27%).[36]

Possible catalytic mechanism

In order to deeply understand the catalytic performance of as-prepared samples, the cumulative amount of ˙OH radicals was measured by photoluminescence (PL) technique with the similar method according to our previous work.[32] The TA solution was selected as a probe molecule to react with ˙OH to produce highly fluorescent product 2-hydroxyterephthalic acid.[10] It can be observed from Fig. 7a that a gradual increase of the PL intensity appears at 445 nm under UV light irradiation with the reaction time, suggesting that fluorescence presents because of the reactions of TA with ˙OH, showing a proportional relationship between PL intensity and the amount of generated ˙OH.[32] Fig. 7b presents a comparison of the PL intensities of RGO/$MnFe_2O_4$-75, $MnFe_2O_4$ and RGO samples in the assistance of H_2O_2. As shown in Fig. 6b, the amount of produced ˙OH radicals by the tested samples decreases in the same order of their MB catalytic performances (RGO/$MnFe_2O_4$-75 > $MnFe_2O_4$ > RGO). This agreement between catalytic performance and hydroxyl radical measurement further clarifies that positive effect between $MnFe_2O_4$ and RGO on the MB decomposition in this study.

The mechanism of the enhanced catalytic performance for RGO/$MnFe_2O_4$ may be explained by the possible electron transfer process of $MnFe_2O_4$ during the reaction. According to the experimental results of XPS analysis, iron and manganese of $MnFe_2O_4$ exist mainly in the oxidation state, *i.e.* Fe(III) and Mn(II), respectively. Thus, Fe_2O_3 and MnO samples were prepared for further analysis (as shown in Sp4†). The catalytic performances of individual Fe_2O_3, MnO and $MnFe_2O_4$ were evaluated under the same condition (Fig. 8a). It is observed that MB decomposition rate is dominated by Fe_2O_3 in the initial stage (<70 min) then by MnO in the later stage (>70 min). As a result, the performance of $MnFe_2O_4$ is superior to that of individual MnO and Fe_2O_3 during the whole process. The competitive PL intensities of MnO and Fe_2O_3 are shown in Fig. 8b–d. The results demonstrate that the performance of above catalysts is related to the amount of ˙OH. In the starting period (20 min), the amount of ˙OH produced by Fe_2O_3 is more than that of MnO (as shown in Fig. 8b), which exhibits a contrary result when the reaction time is more than 70 min (Fig. 8c and d). The amount of ˙OH produced by $MnFe_2O_4$ is larger than those of MnO and Fe_2O_3 in the whole process, which are in good agreement with their catalytic performances as described in Fig. 8a.

The performance of Fe_2O_3 may be attributed to the significant effect of Fe^{3+}/Fe^{2+} cycling to yield ˙OH radicals for the degradation of organic pollutants. At first, Fe^{3+} is reduced to Fe^{2+} which subsequently reacts with H_2O_2 to produce ˙OH and Fe^{3+}. Consequently, such process accelerates the Fe^{3+}/Fe^{2+} cycle to form the large amount of strong oxidant ˙OH for the degradation of MB.[27,47] The main process may be described as eqn (1) and (2).

$$Fe^{3+} + H_2O_2 \rightarrow Fe^{2+} + {}^{\cdot}OOH + H^+ \quad (1)$$

$$Fe^{2+} + H_2O_2 \rightarrow Fe^{3+} + {}^{\cdot}OH + OH^- \quad (2)$$

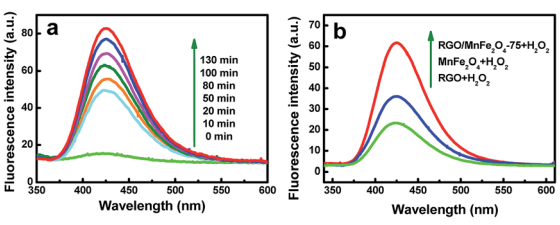

Fig. 7 (a) PL spectra of 5×10^{-4} M basic TA solution treated by RGO/$MnFe_2O_4$-75 irradiated by UV light under different time (excitation at 325 nm) and (b) PL spectra of 5×10^{-4} M basic TA solution treated by various samples irradiated by UV light at 50 min.

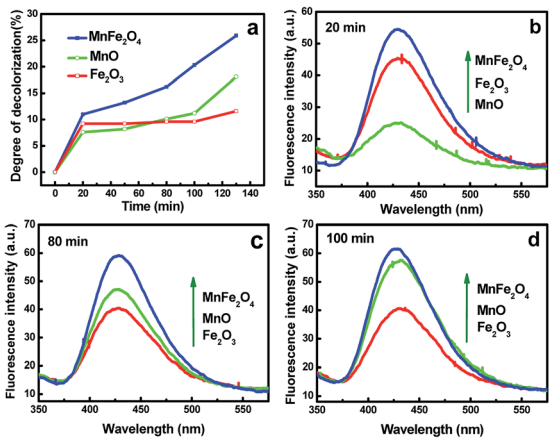

Fig. 8 (a) Time profiles of MB decolorization (50 mg L^{-1}, 10 mL) treated by different samples under the same condition; (b–d) PL spectra of various samples in a 5×10^{-4} M basic TA solution under UV light irradiation.

The reactions between Mn^{2+} and H_2O_2 can also contribute to the generation of $^{\cdot}OH$, which would be responsible for the remarkable increase on the catalytic activities,[46] as shown in eqn (3) and (4).

$$Mn^{2+} + H_2O_2 \rightarrow Mn^{3+} + {}^{\cdot}OH + OH^- \quad (3)$$

$$Mn^{3+} + H_2O_2 \rightarrow Mn^{2+} + {}^{\cdot}OOH + H^+ \quad (4)$$

Beside the Fe^{3+}/Fe^{2+} and Mn^{3+}/Mn^{2+} cycles, the reaction between Fe^{2+} and Mn^{3+} is thermodynamically favorable, which benefits the redox cycles of Fe^{3+}/Fe^{2+} ($E^{\theta}(Fe^{3+}/Fe^{2+}) = 0.77$ V) and Mn^{3+}/Mn^{2+} ($E^{\theta}(Mn^{3+}/Mn^{2+}) = 1.51$ V) (as shown in eqn (5)).

$$Fe^{2+} + Mn^{3+} \rightarrow Fe^{3+} + Mn^{2+},\ E^{\theta} = 0.74\ V \quad (5)$$

Given the better catalytic performance of $MnFe_2O_4$ than those of individual Fe_2O_3 and MnO, it is anticipated that the synergetic effects of the redox couples of Mn^{3+}/Mn^{2+}, Fe^{3+}/Fe^{2+} and Fe^{2+}/Mn^{3+} during the reaction is responsible for the enhanced performance.

In order to further demonstrate the oxidation state of Mn and Fe of $MnFe_2O_4$ during the reaction, XPS spectra of the cycled RGO/$MnFe_2O_4$-75-R were further recorded (see Sp5†). Comparing to the Mn 2p and Fe 2p in Fig. 3b and c, the RGO/$MnFe_2O_4$-75-R hybrid exists the same peaks with the fresh one. However, there are some slight differences of the binding energies and the full widths at half maximum (FWHM) values of Fe 2p as well as Mn 2p before and after Fenton reaction, which have been displayed in Tables S1 and S2,† respectively. Such results may be attributed to the electron transfer of Fe^{3+}/Fe^{2+} and Mn^{3+}/Mn^{2+} in the catalytic process. H_2-TPR measurement was further applied in the $MnFe_2O_4$ catalyst with Mn_3O_4 and Fe_2O_3 as the references (Sp6†). It is found that the reduction step of Fe^{3+} to Fe^{2+} starts at a higher temperature (320 °C) comparing with that of Mn^{3+} to Mn^{2+} (210 °C).[48] This observation suggests that Mn^{3+}/Mn^{2+} presents higher oxidation capacity than Fe^{3+}/Fe^{2+}, which is in agreement the reaction described in eqn (5).

Accordingly, the mechanism schematic of MB decomposition on RGO/$MnFe_2O_4$ catalyst with the assistance of H_2O_2 was shown in Fig. 9. At first, MB molecules are adsorbed on the RGO and its giant π-conjugation system and 2D planar structure help to promote the electron transfer during the catalytic reaction.[32,49] Besides, $MnFe_2O_4$ nanoparticles anchored on the RGO surface catalyze H_2O_2 to produce large amount of $^{\cdot}OH$ radicals and constantly facilitate the decomposition of MB molecules into CO_2, H_2O and SO_4^{2-} *etc.* During the catalytic process, the coexistence of the internal electron transfer in Fe^{3+}/Fe^{2+} and Mn^{3+}/Mn^{2+} redox couples have prominent contributions to the significant catalytic performance, wherein the former help to that of the earlier 70 min and the later plays a positive role in the last period. Furthermore, the reduction of Mn^{3+} by Fe^{2+} during the reaction is thermodynamically favorable, which in turn benefits the redox cycles of Fe^{3+}/Fe^{2+} and Mn^{3+}/Mn^{2+}. Therefore, the coupling contributions of RGO/$MnFe_2O_4$ catalyst result in an appreciable improvement in the decomposition of MB.

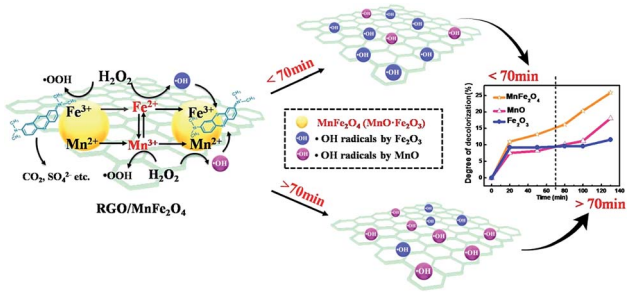

Fig. 9 Schematic of the mechanism of MB decomposition on RGO/$MnFe_2O_4$ hybrid with the assistance of H_2O_2.

Conclusions

In summary, we have successfully synthesized magnetic RGO/$MnFe_2O_4$ hybrids with pristine GO/$MnSO_4$ suspension derived from a modified Hummers method and ferrous sulfate as the main precursors. Such a process not only alleviates the tedious purification process for GO production, but also contributes to a high atom-economic synthesis. The combination of magnetic $MnFe_2O_4$ particles with RGO plays an important role in controlling the size and distribution of the $MnFe_2O_4$ nanoparticles, thus allowing excellent catalytic performance for the decomposition of MB. In particular, MB dye molecules in neutral solution can be fully decomposed within 130 min in the presence of H_2O_2 at room temperature. The sequential synergetic actions of Fe^{3+}/Fe^{2+}, Mn^{3+}/Mn^{2+} and Fe^{2+}/Mn^{3+} redox couples at different stages contribute to the excellent catalytic activity. Besides, the magnetic property of the $MnFe_2O_4$ nanoparticles greatly simplifies the recycling performance. This work not only offers a new approach to fabricate graphene-based functional hybrids, but also benefits understanding the mechanism of transition metals on the heterogeneous Fenton system.

Acknowledgements

This work is supported by the NSFC (No. 51372277, 50902066), China Postdoctoral Science Foundation (2013M530922, 2014T70253), Program for Liaoning Excellent Talents in University (LJQ2014118), the Fundamental Research Funds for the Central Universities (No. 15CX08005A), Natural Science Fund of Liaoning Province (201602458).

References

1 N. N. Tušar, D. Maučec, M. Rangus, I. Arčon, M. Mazaj, M. Cotman, A. Pintar and V. Kaučič, *Adv. Funct. Mater.*, 2012, **22**, 820–826.
2 B. Jiang, Y. Liu, J. Zheng, M. Tan, Z. Wang and M. Wu, *Environ. Sci. Technol.*, 2015, **49**, 12363–12371.
3 B. Jiang, X. Wang, Y. Liu, Z. Wang, J. Zheng and M. Wu, *J. Hazard. Mater.*, 2016, **304**, 457–466.
4 M. Munoz, Z. M. de Pedro, J. A. Casas and J. J. Rodriguez, *Appl. Catal., B*, 2015, **176–177**, 249–265.

5 S. Navalon, M. Alvaro and H. Garcia, *Appl. Catal., B*, 2010, **99**, 1–26.
6 M. Cheng, G. Zeng, D. Huang, C. Lai, P. Xu, C. Zhang and Y. Liu, *Chem. Eng. J.*, 2016, **284**, 582–598.
7 Y. L. Pang, S. Lim, H. C. Ong and W. T. Chong, *Ceram. Int.*, 2016, **42**, 9–34.
8 T. Zeng, W. Chen, C. M. Cirtiu, A. Moores, G. Song and C. Li, *Green Chem.*, 2010, **12**, 570–573.
9 B. Wang, H. Wu, L. Yu, R. Xu, T. T. Lim and X. W. Lou, *Adv. Mater.*, 2012, **24**, 1111–1116.
10 L. Zhang, Y. Nie, C. Hu and X. Hu, *J. Hazard. Mater.*, 2011, **190**, 780–785.
11 T. Rhadfi, J. Y. Piquemal, L. Sicard, F. Herbst, E. Briot, M. Benedetti and A. Atlamsani, *Appl. Catal., A*, 2010, **386**, 132–139.
12 Y. Zhong, X. Liang, Z. He, W. Tan, J. Zhu, P. Yuan, R. Zhu and H. He, *Appl. Catal., B*, 2014, **150–151**, 612–618.
13 Y. Guo, L. Zhang, X. Liu, B. Li, D. Tang, W. Liu and W. Qin, *J. Mater. Chem. A*, 2016, **4**, 4044–4055.
14 H. Z. P. M. Rice, S. X. Wang and S. Sun, *J. Am. Chem. Soc.*, 2004, **126**, 11458–11459.
15 P. Deng, F. Mou, X. Li, Z. Deng, J. Sun, L. Xu and J. Guan, *J. Mater. Chem. A*, 2016, **4**, 11768–11774.
16 D. Vilela, J. Parmar, Y. Zeng, Y. Zhao and S. Sanchez, *Nano Lett.*, 2016, **16**, 2860–2866.
17 X. Fang, J. Xiao, S. Yang, H. He and C. Sun, *Appl. Catal., B*, 2015, **162**, 544–550.
18 L. Yang, Y. Zhang, X. Liu, X. Jiang, Z. Zhang, T. Zhang and L. Zhang, *Chem. Eng. J.*, 2014, **246**, 88–96.
19 G. Chen, J. Wang, L. Zhou, W. Ma, D. Zhang, F. Ren, H. Yan, G. Qiu, X. Liu and P. Joy, *J. Am. Ceram. Soc.*, 2012, **95**, 3569–3576.
20 J. Gu, X. Yang, Z. Lv, N. Li, C. Liang and Q. Zhang, *Int. J. Heat Mass Transfer*, 2016, **92**, 15–22.
21 H. Gu, C. Ma, J. Gu, J. Guo, X. Yan, J. Huang, Q. Zhang and Z. Guo, *J. Mater. Chem. C*, 2016, **4**, 5890–5906.
22 J. Gu, N. Li, L. Tian, Z. Lv and Q. Zhang, *RSC Adv.*, 2015, **5**, 36334–36339.
23 J. Gu, C. Xie, H. Li, J. Dang, W. Geng and Q. Zhang, *Polym. Compos.*, 2013, **35**, 1087–1092.
24 A. K. Geim, *Science*, 2009, **324**, 1530–1534.
25 B. Xia, Y. Yan, X. Wang and X. W. Lou, *Mater. Horiz.*, 2014, **1**, 379–399.
26 H. Hu, Z. Zhao, Y. Gogotsi and J. Qiu, *Environ. Sci. Technol. Lett.*, 2014, **1**, 214–220.
27 S. Han, L. Hu, Z. Liang, S. Wageh, A. A. Al-Ghamdi, Y. Chen and X. Fang, *Adv. Funct. Mater.*, 2014, **24**, 5719–5727.
28 S. Bai, X. Shen, X. Zhong, Y. Liu, G. Zhu, X. Xu and K. Chen, *Carbon*, 2012, **50**, 2337–2346.
29 Y. Yao, Y. Cai, F. Lu, F. Wei, X. Wang and S. Wang, *J. Hazard. Mater.*, 2014, **270**, 61–70.
30 W. Zhao, J. Kong, H. Liu, Q. Zhuang, J. Gu and Z. Guo, *Nanoscale*, 2016, DOI: 10.1039/c6nr06622d.
31 J. Qu, L. Shi, C. He, F. Gao, B. Li, Q. Zhou, H. Hu, G. Shao, X. Wang and J. Qiu, *Carbon*, 2014, **66**, 485–492.
32 Y. Li, J. Qu, F. Gao, S. Lv, L. Shi, C. He and J. Sun, *Appl. Catal., B*, 2015, **162**, 268–274.
33 J. Qu, F. Gao, Q. Zhou, Z. Wang, H. Hu, B. Li, W. Wan, X. Wang and J. Qiu, *Nanoscale*, 2013, **5**, 2999–3005.
34 L. L. Peng, X. Peng, B. R. Liu, C. Z. Wu, Y. Xie and G. H. Yu, *Nano Lett.*, 2013, **13**, 2151–2157.
35 H. Hu, Z. Zhao, Q. Zhou, Y. Gogotsi and J. Qiu, *Carbon*, 2012, **50**, 3267–3273.
36 N. Li, Z. F. Geng, M. H. Cao, L. Ren, X. Y. Zhao, B. Liu, Y. Tian and C. W. Hu, *Carbon*, 2013, **54**, 124–132.
37 Y. L. Xiao, J. T. Zai, L. Q. Tao, B. Li, Q. Y. Han, C. Yu and X. F. Qian, *Phys. Chem. Chem. Phys.*, 2013, **15**, 3939–3945.
38 D. C. Hong, Y. Yamada, T. Nagatomi, Y. Takai and S. Fukuzumi, *J. Am. Chem. Soc.*, 2012, **134**, 19572–19575.
39 Y. S. Fu, P. Xiong, H. Q. Chen, X. Q. Sun and X. Wang, *Ind. Eng. Chem. Res.*, 2012, **51**, 725–731.
40 Y. Zhou, B. Xiao, S. Q. Liu, Z. Meng, Z. G. Chen, C. Y. Zou, C. B. Liu, F. Chen and X. Zhou, *Chem. Eng. J.*, 2016, **283**, 266–275.
41 J. Gu, C. Liang, J. Dang, W. Dong and Q. Zhang, *RSC Adv.*, 2016, **6**, 35809–35814.
42 J. Zhu, S. Wei, H. Gu, S. B. Rapole, Q. Wang, Z. Luo, N. Haldolaarachchige, D. P. Young and Z. Guo, *Environ. Sci. Technol.*, 2012, **46**(2), 977–985.
43 Z. Bai, B. Sun, N. Fan, Z. Ju, M. Li, L. Xu and Y. Qian, *Chem.–Eur. J.*, 2012, **18**, 5319–5324.
44 J. Chun, H. Lee, S. H. Lee, S. W. Hong, J. Lee, C. Lee and J. Lee, *Chemosphere*, 2012, **89**, 1230–1237.
45 R. C. Costa, M. F. Lelis, L. C. Oliveira, J. D. Fabris, J. D. Ardisson, R. R. Rios, C. N. Silva and R. M. Lago, *J. Hazard. Mater.*, 2006, **129**, 171–178.
46 R. C. Costa, M. F. Lelis, L. C. Oliveira, J. D. Fabris, J. D. Ardisson, R. R. Rios, C. N. Silva and R. M. Lago, *Catal. Commun.*, 2003, **4**, 525–529.
47 S. Guo, G. Zhang, Y. Guo and J. C. Yu, *Carbon*, 2013, **60**, 437–444.
48 Y. Wang, H. Zhao, M. Li, J. Fan and G. Zhao, *Appl. Catal., B*, 2014, **147**, 534–545.
49 L. Zhang, Q. Zhang, H. Xie, J. Guo, H. Lyu, Y. Li, Z. Sun, H. Wang and Z. Guo, *Appl. Catal., B*, 2017, **201**, 470–478.